Analysis of in-silico Body Surface P-wave Integral Maps show Important Differences depending on the Connections between Coronary Sinus and Left Atrium

*Ana Ferrer-Albero[1], Eduardo J Godoy[2], Rafael Sebastian[2], Laura Martínez[1], Javier Saiz[1]

[1]Universitat Politècnica de Valencia, Valencia, Spain
[2]Universitat de Valencia, Valencia, Spain

Abstract

The electrical connections between the atrial coronary sinus (CS) and the left atrial (LA) myocardium have an effect on the overall atrial activation pattern and the P-wave morphology. In this study, we use our validated multi-scale 3D human atrial-torso model to elucidate which electro-anatomical configuration of connections between CS and LA more accurately reproduces a set of body surface P-wave integral maps (BSPiM) acquired in the clinic. We performed atrial biophysical simulations by pacing in distal and proximal LA sites. The corresponding in-silico BSPiM were then computed and compared with published clinical patterns obtained from patients.

Important differences in BSPiM were observed depending on the presence or absence of CS-LA electrical connections. Furthermore, when these junctions exist, the patterns slightly differ among themselves depending on their distal or proximal location with respect to the ostium of the CS.

1. Introduction

Body surface potential mapping (BSPM) systems offer non-invasive ways to explore the behaviour of the atria. However, it is still very difficult to determine the specific location of ectopic foci when disturbances appear on the recorded signals by only analysing the BSPM. Instead, some experimental studies [1,2] have built and exploited a database of clinical patterns obtained from patients who underwent paced mapping before a diagnostic electrophysiological study. These patterns correspond to body surface P-wave integral maps (BSPiM) where ectopic beats are paced in different atrial sites, and are used to infer how the atria is really activating and how its electrical contribution is observed on the torso surface. This indicator is well correlated with P-wave polarity and amplitude and more importantly, it is robust against fast polarity changes and interpatient variability. To be able to get insight into those clinical studies, biophysical models can be used to analyse the relationship between ectopic atrial activity and BSPiM. However, it requires a very accurate atrial model capable of reproducing existing clinical measurements. This atrial model must include all the anatomical regions to allow the electrical wavefront propagates following muscular connections.

In this respect, several clinical studies of the human atria have histologically shown the existence of striated myocardial muscle at discrete locations along the sleeve of the coronary sinus (CS) that electrically connects CS and the left atrial (LA) myocardium [3,4]. The anatomy of these interatrial connections and their location have been previously shown as having high variability between patients. This leads to strong differences in the pathway followed by the atrial depolarization wavefront [3] and influences the BSPiM.

Up to now, there is no consensus on the number and location of these muscular connections so 3D computational models of the human atrial anatomy and electrophysiology have not historically included the CS and its bridges to LA as an essential region responsible for the depolarization atrial pattern [5-8]. However, the influence of these bridges on the depolarization wavefront were partly taken into account in the multi-scale 3D human atrial-torso models previously developed by our group [9,10].

The present study combines our most recent multi-scale 3D human atrial-torso model [9] with the analysis of BSPiMs with the aim of determining which configuration of the CS-LA connections reproduces more accurately the set of clinically observed body surface P-wave integral maps (BSPiM).

2. Material and methods

2.1 Anatomical multi-scale model

Our 3D human atrial model consists of a computational finite element mesh with a homogeneous wall thickness between 600 and 900 μm (754.893 nodes and 515.005 elements), built with linear hexahedral elements and with

a regular spatial resolution of 300 µm (Figure 1). The torso model developed in [9] was re-meshed to improve the spatial resolution in the endocardium-blood interface to enhance the accuracy in the region where the atrial and torso models couples. The resulting volumetric mesh has 254.976 nodes and 1.554.255 tetrahedral elements. The mesh spatial resolution ranges approximately from 0.5 mm on the atrial endocardium-blood interface to 5.8 mm on the torso surface. Six different regions (lung, bone, liver, ventricle, blood, and general torso) with their corresponding tissue conductivities associated to the torso elements were defined.

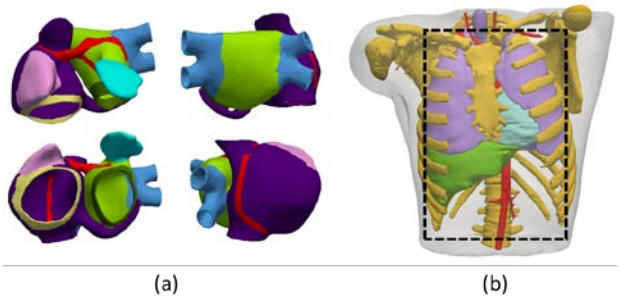

Figure 1: a) colour-coded atria model depending on the region with different electrical properties; b) torso model including regions. Dotted square on the torso surface defines the frontal and rear views of the torso where P waves are computed.

2.2 Biophysical simulations

The Courtemanche-Ramírez-Nattel (CRN) ionic model for human atrial electrophysiology was used to simulate the action potentials [11]. Nine cellular models of atrial myocytes were considered by adjusting the original model parameters at several regions. Heterogeneous atrial tissue properties were also set in different anatomical regions (Figure 1a) as defined in [9].

The electrical propagation was performed by using the mono-domain approach and the finite element method [12] to solve the reaction-diffusion system described by equations (1) and (2) and to provide the transmembrane potential (V_m). Then, the extracellular potentials (V_e) were computed by an approximation of the bi-domain approach. Firstly, we interpolate the transmembrane potentials obtained in the atrial hexahedral mesh to the atrial nodes of the torso model (tetrahedral mesh). Secondly, the propagation from the atria to torso surface was performed by solving the passive term of the bi-domain model, equation (3), using again the finite elements method and Dirichlet and Neumann boundary conditions [13],

$$\nabla \cdot (\boldsymbol{D}\nabla V) = C_m \cdot \frac{\partial V_m}{\partial t} + I_{ion} \; in \; \Omega_H \qquad (1)$$

$$\mathbf{n} \cdot (\boldsymbol{D}\nabla V) = 0 \; in \; \partial\Omega_H \qquad (2)$$

$$\nabla \cdot (\boldsymbol{D_i}\nabla V_m) + \nabla \cdot ((\boldsymbol{D_i} + \boldsymbol{D_e})\nabla V_e) = 0 \qquad (3)$$

where D is the equivalent conductivity tensor, D_i and D_e are the volume-averaged conductivity tensors of the intra- and extracellular domains, V_m is the transmembrane potential, I_{ion} is the transmembrane ionic current that depends on the cellular model, C_m is the membrane capacitance and Ω_H is the heart domain

The stimulation protocol consisted of a model stabilization phase (in 3D with all regional models coupled) of 20 continuous beats with a basic cycle length (BCL) of 500ms, followed by an additional beat with the same BCL paced at distal and proximal LA distinct sites. Two different anatomical configurations were simulated by blocking or allowing the electrical communication in the junction at distal and proximal LA pacing sites towards the CS (4 independent simulations were performed).

Pacing sites were selected as shown in Figure 3 row 1: low LA, at the farthest point from the ostium of CS, considering the CS-LA electrical junction activated (Figure 3a) or blocked (Figure 3b); low LA, at the closest point from the ostium, considering the CS-LA electrical junction activated (Figure 3c) or blocked (figure 3d).

2.3 Body surface P-wave integral maps

Simulated electrocardiographic P-waves were registered at the torso surface nodes (14.157 leads) to build the body surface potential distribution (BSPM). Afterwards, the time integral patterns were computed from the P-wave measured at each lead (BSPiM). These integral maps represent the area under the P-wave, between the zero line and the curve outlined from the P-wave onset to its offset. These two fiducial points were defined as the time instant at which the atrial depolarization starts from the ectopic foci and the time instant at which the latest atrial node is already depolarized, respectively.

The P-wave integral maps were displayed in the form of positive-negative maps where the zero iso-integral line divides those areas of the torso surface where P-waves are positive signed from those with negative morphology (Figure 2).

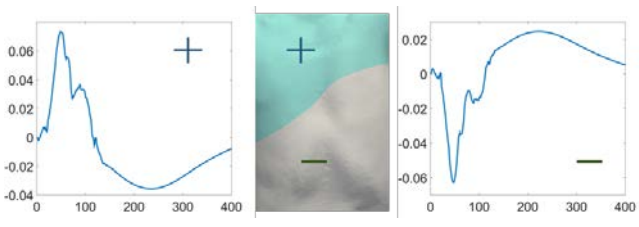

Figure 2: Characteristic P-wave integral map (BSPiM) (centre). Bluish area represents positive P-waves (leftwards), registered at any lead of this area, and greyish region means negative P-waves (rightwards).

3. Results

Local activation times (LATs) were obtained after simulating the last ectopic beat as described in section 2.2. Figure 3 row (2) displays the LATs produced by each configuration. Figure 3a shows how the wavefront propagation starts depolarizing the LA upwards but entering very fast to the RA through the CS and then depolarizing upwards this atrium almost simultaneously. Figure 3b outlines the same depolarization profile for LA, but in the opposite direction in the case of RA since the wavefront enters though the Bachmann Bundle instead of using the CS-LA junctions. Similar effect is shown when the pacing site is near the ostium of CS. When the CS-LA junction is electrically activated (see Figure 3c) both atria depolarize upwards thanks to the fast connection between LA and RA. However, when this bridge is blocked (d), the two atria depolarize in opposite direction as happens in configuration (b).

In-silico BSPiMs shown in Figure 3 row (3), consist of two ROIs (see Figure 1b, slashed-line) from the frontal (left) and rear (right) views of the torso surface. The BSPiM produced when the potential wavefront enters through distal muscular CS-LA connections (a), shows that P-wave morphology is positively signed mainly on the right side of the torso surface corresponding to the frontal-superior side and to the right-superior corner at the back. However, when the wavefront does not find distal muscular CS-LA bridges (b), the positive P-wave integral pattern appears on the inferior part of the torso in both torso faces. Simulations with proximal CS-LA connections (c) show patterns inverted with respect to the configuration without them (d). The patterns associated to models with no proximal or distal CS-LA connections (b, d) are similar among themselves but opposite to the configurations when bridges CS-LA (a, c) are activated.

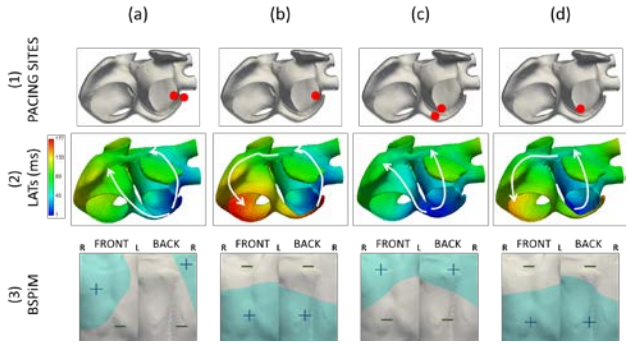

Figure 3: In-silico simulations when foci are paced in distal, (a, b), and proximal, (c, d), LA sites. Row (1): Double-red dots represent a bridge between CS and LA myocardium, (a, c). Single-red dots, (b, d), represent the lack of CS-LA connections. Row (2): LATs for each configuration with arrows showing the direction of the depolarization wavefront. Row (3): In-silico BSPiMs. Bluish areas represent positive signed BSPiMs while greyish areas represent those with negative signed BSPiMs. R and L identify the right and left sides of the frontal and rear views of the torso surface.

In-vivo clinical BSPiMs described in [2,14] show similar behaviour. In these studies, the authors recorded sixty-two-lead body surface ECG recordings during LA pace mapping in 22 patients with normal cardiac anatomy. The results obtained when pacing at low LA are depicted in Figure 4 for points 10 to 13. The farthest point from the ostium of CS corresponds to the site number 10, which BSPiMs is highly similar to our pattern showed in Figure 3, row 3(a). Furthermore, the sites from 11 to 13 describe a positive signed integral map on the superior part of frontal and rear part of the torso surface while it is negative underneath. These three patterns closely match our in-silico BSPiMs depicted in Figure 3, row 3(c).

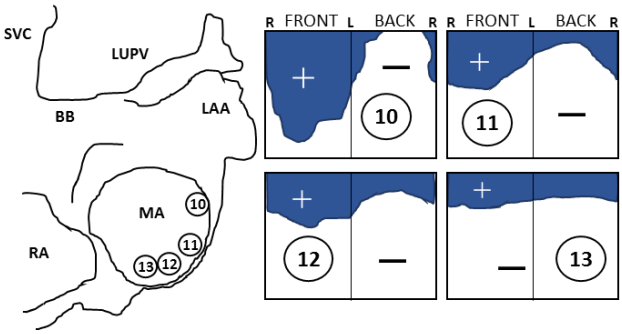

Figure 4: In-vivo clinical BSPiMs reproduced from the originals published in [2,14]. Bluish areas represent positive signed P-wave integrals while whitish are negative signed. R and L identify the right and left sides of the frontal and rear views of the torso surface.

4. Discussion and conclusions

This study demonstrates the relevance of including and realistically modelling the striated myocardial muscle connections between CS and LA. These bridges allow the electrical wavefront initiated in the low LA to enter the RA underside through the CS and depolarized both atria upwards. The effect that these bridges have on the morphology of the P-wave when registering the ECG on the torso surface is key. Hence, when the junctions are blocked, the P-wave integral maps describe always the same pattern: positive underneath and negative above. However, if the bridges are working properly, the patterns are completely opposite, with positive integrals above and negative below. Small differences in this last configuration mainly depend on how far or close are both, the pacing site and the bridge from the ostium of the CS.

The results obtained when comparing our in-silico patterns and experimental studies previously performed [2,14] demonstrate that only when electrical junctions are activated the patterns match closely. However, a more in depth analysis has yet to be done regarding the number a location of the in-silico CS-LA connections. We might hypothesize that including additional bridges close to the CS ostium could produce P-wave integral patterns different from those simulated in this work.

In conclusion, since previous computational 3D human atrial and torso models [5-8] lack these muscular connections, the present analysis shows the importance of taking into account this CS-LA connection. The multi-scale model provided [9] could be very useful to study the spatial origin of ectopic atrial excitations, atrial arrhythmias or any other pathological atrial condition with a more curate methodology.

Acknowledgements

This work was partially supported by the "VI Plan Nacional de Investigación Científica, Desarrollo e Innovación Tecnológica" from the Ministerio de Economía y Competitividad of Spain and the European Commission (European Regional Development Funds - ERDF - FEDER), Award Number: TIN2012-37546-C03-01; the "Programa Estatal de Investigación, Desarrollo e Innovación Orientado a los Retos de la Sociedad" from the Ministerio de Economía y Competitividad and the European Commission (European Regional Development Funds - ERDF - FEDER), Award Number: TIN2014-59932-JIN; and the "Programa Prometeo" from the Generalitat Valenciana, Award Number: 2012/030.

References

[1] SippensGroenewegen A, Peeters HA, Jessurun ER, Linnenbank AC, Robles de Medina EO, Lesh MD, et al. Body surface mapping during pacing at multiple sites in the human atrium: P-wave morphology of ectopic right atrial activation. Circulation 1998;97:369–80.

[2] SippensGroenewegen A, Natale A, Marrouche NF, Bash D, Cheng J. Potential role of body surface ECG mapping for localization of atrial fibrillation trigger sites. J Electrocardiol 2004;37:47–52.

[3] Chauvin M, Shah DC, Haïssaguerre M, Marcellin L, Brechenmacher C. The anatomic basis of connections between the coronary sinus musculature and the left atrium in humans. Circulation 2000;101:647–52. doi:10.1161/01.CIR.101.6.647.

[4] Saremi F, Thonar B, Sarlaty T, Shmayevich I, Malik S, Smith CW, et al. Posterior Interatrial Muscular Connection between the Coronary Sinus and Left Atrium: Anatomic and Functional Study of the Coronary Sinus with Multidetector CT. Radiology 2011;260:671–9.

[5] Burdumy M, Luik A, Neher P, Hanna R, Krueger MW, Schilling C, et al. Comparing measured and simulated wave directions in the left atrium a workflow for model personalization and validation. Biomed Tech 2012;57:79–87.

[6] McDowell KS, Vadakkumpadan F, Blake R, Blauer J, Plank G, MacLeod RS, et al. Methodology for patient-specific modeling of atrial fibrosis as a substrate for atrial fibrillation. J Electrocardiol 2012;45:640–5.

[7] Deng D, Jiao P, Ye X, Xia L. An image-based model of the whole human heart with detailed anatomical structure and fiber orientation. Comput Math Methods Med 2012;2012:891070.

[8] Krueger MW, Seemann G, Rhode K, Keller DUJ, Schilling C, Arujuna A, et al. Personalization of atrial anatomy and electrophysiology as a basis for clinical modeling of radio-frequency ablation of atrial fibrillation. IEEE Trans Med Imaging 2013;32:73–84.

[9] Ferrer A, Sebastián R, Sánchez-Quintana D, Rodríguez JF, Godoy EJ, Martínez L, et al. Detailed Anatomical and Electrophysiological Models of Human Atria and Torso for the Simulation of Atrial Activation. PLoS One 2015;10:e0141573.

[10] Tobón C, Ruiz-Villa C a., Heidenreich E, Romero L, Hornero F, Saiz J. A Three-Dimensional Human Atrial Model with Fiber Orientation. Electrograms and Arrhythmic Activation Patterns Relationship. PLoS One 2013;8:e50883.

[11] Courtemanche M, Ramirez RJ, Nattel S. Ionic mechanisms underlying human atrial action potential properties: insights from a mathematical model. Am J Physiol 1998;275:H301–21.

[12] Heidenreich EA, Ferrero JM, Doblaré M, Rodríguez JF. Adaptive macro finite elements for the numerical solution of monodomain equations in cardiac electrophysiology. Ann Biomed Eng 2010;38:2331–45.

[13] Weber FM, Keller DUJ, Bauer S, Seemann G, Lorenz C, Dössel O. Predicting tissue conductivity influences on body surface potentials-An efficient approach based on principal component analysis. IEEE Trans Biomed Eng 2011;58:265–73.

[14] Groenewegen AS. Non-invasive localization and treatment of focal atrial fibrillation, 2004.

Address for correspondence:

Ana Ferrer-Albero
Centro de Investigación e Innovación en Bioingeniería (Ci2B). Universidad Politécnica de Valencia. Ciudad Politécnica de la Innovación - Cubo Azul - Edif. 8B- Acceso N. Camino de Vera s/n, 46022. Valencia (España)
anferal0@upvnet.upv.es